TR 116

SEDIMENTATION IN AN ISOLATED INTERDOMAL INTRASLOPE BASIN

by

E. William Behrens

University of Texas Institute for Geophysics
Technical Report 116

submitted to Marine Geology
25 April 1994

Sedimentation in an isolated interdomal intraslope basin

E. William Behrens
Institute for Geophysics, The University of Texas at Austin, 8701 N. Mopac Expressway, Austin, TX 78759-8397

ABSTRACT

Late Quaternary sedimentation and seismic stratigraphy of an intraslope, interdomal basin show both differences and similarities to basins involved in down-slope sediment transport. The basin is both silled and isolated by salt structures from sediments transported down-slope from the shelf. Yet, the basin has a significantly expanded section relative to hemipelagic drape over adjacent bathymetric highs. The expansion results from redistribution of hemipelagic muds into debrites and turbidites which form distinct acoustic and sedimentary facies in the lower basin margin and basin floor respectively. Redeposition thickens the basin fill cyclically, similarly to basins receiving shelf sediments.

Introduction

Objectives

The continental slope in the northwestern Gulf of Mexico is severely deformed by salt tectonics. One result of this is a large number (~100) of isolated to semi-isolated sedimentary and bathymetric intraslope basins each of which may be considered as a sedimentological experiment for the researcher to decipher. In order to organize these experiments into related categories, Bouma and others (in several publications, e.g., Bouma et al., 1978; Bouma and Garrison, 1979; Bouma, 1981; Martin and Bouma, 1981; and Bouma, 1983) have hypothesized two major modes of intraslope basin formation in this region. Gyre Basin (Fig. 1) has been cited as an example of an intraslope basin formed by salt diapirism blocking a submarine canyon (a blocked-canyon basin; Bouma et al., 1978; Bouma, 1983). Orca Basin (Fig. 1) has been cited as an example of a basin formed by simple salt evacuation into diapiric structures which form surrounding bathymetric highs (an interdomal basin; Bouma, 1983).

Limited documentation of these models makes it important for further studies to test and evaluate them. For example, a preexisting canyon has not been shown for Gyre Basin. Nearby, Satterfield and Behrens (1990) have provided an alternative model for downslope transport of shelf sediment into a succession of pre-existing intraslope basins through a series of submarine canyons and channels. In the case of Orca Basin, 200 meters of brine accumulating in it through the Holocene make it unique in many ways (Trabant and Presley, 1978; Bouma et al. 1986), and thus, by definition, not typical.

This paper provides documentation of the geologic setting and sedimentary processes and products within an isolated, interdomal intraslope

basin. Although isolated from an input of shelf sediments, the basin does contain turbidity current and debris flow deposits (turbidites and debrites). Thus the basin provides a record of mass transport and implied slope instability reflecting salt tectonism rather than sea level effects on the shelf edge.

Location

The basin studied is roughly circular and centered at 27°07'N and 94°45'W (Figs. 1 & 2). Surrounding water depths are about 1100 m, and the basin floor reaches almost 1800 m. The basin is shown by Satterfield and Behrens (1990; Basin V, Figure 1) to be just beyond (downslope and isolated from) the canyon/channel system involved in turbidite redeposition of sandy shelf sediments in a downslope succession of intraslope basins. It is 28 km (15 n.mi.) southwest of Gyre Basin.

Data

The data base for this study includes over 330 km (180 n.mi.) of high frequency (3.5 kHz) reflection profiles, two 24-channel reflection lines, and nine piston cores (Fig. 2a). Cores were analyzed regularly (20 cm intervals) for water content (porosity) and calcium carbonate and irregularly for textures and stable carbon isotopes of organic carbon in addition to routine visual logging of sediment types and structures. Porosity was calculated from evaporative water loss (Behrens, 1980). Carbonate was determined by weight loss from acidification (HCl). Textures were determined by wet sieving and pipette analyses (4 to 12 phi).

The data were acquired on eight cruises of the R/Vs FRED H. MOORE (1980, 1985 and 1986), IDA GREEN (1976, 1981 and 1982), GYRE (1989) and LONGHORN (1990). All navigation was LoranC acquired with the same instrument (a Northstar 6000), the locations from which are offset approximately 0.5 km southeast of GPS values.

Observations

Morphology and echo character

The basin has an area of approximately 260 km^2 (76 square nautical miles) which is about average for central slope basins. Three roughly concentric, bathymetric zones can be distinguished - 1) steep basin margin, 2) lower basin margin, and 3) basin floor - and each zone has distinctive acoustic reflection characteristics (Table 1; Figs. 2b and 3).

About 69% of the basin consists of steep (e.g., 8°) margins which may reflect little or no energy vertically, show a thin bottom reflection, or sometimes resolve into many, parallel subbottom reflections (Fig. 3; Type I of

Satterfield and Behrens, 1990). The width of the zone ranges from 2.5 to 6.5 km and averages about 3.5 km (range: 1.3 - 3.5 n.mi., av..: 2 n.mi.).

The lower basin margin constitutes about 25% of the basin and is characterized by hummocky, diffuse bottom echoes with few if any sub-bottom reflections (Fig. 3; Type V of Satterfield and Behrens, 1990). The width ranges from 1.5 to 5.5 km and averages 2.5 km (0.8 - 3, and 1.3 n.mi. respectively).

The basin floor makes up only 6% of the basin and has a sharp bottom echo with a few (3 - 5) subparallel subbottom reflections (Fig. 3; Type II of Satterfield and Behrens, 1990). The width (diameter) of the basin floor ranges from about 3 to 5.5 km and averages about 3.5 km (1.6 - 3, and 2 n.mi. respectively). The boundaries of these zones tend to be broadly parallel (Fig. 2b).

Sediments

Three common sediment types are observed in cores from the basin: hemipelagic mud, debrites, and turbidites. Appendix A lists textural characteristics of these and some related sediments.

Hemipelagic mud

Cores from bathymetric highs, which can receive only sediment settling from suspension, typically have had all traces of bedding destroyed by bioturbation which is manifest as a considerable variety of indistinct to distinct mottles. This material is abundant, especially in the upper parts of cores from the basin. Clays make up over 80% of most samples, with particles finer than 10 phi making up about 60% and particles finer than 12 phi making up roughly 25%. The resultant mean grain sizes are generally a little over 10 phi. Although very fine grained, these sediments always contain some (e.g., 1 - 3 %) sand-sized grains of skeletal carbonate.

A variety of subtle shades of olive grey colors and mottle types often follow a stratigraphically correlatable sequence in cores from the midslope region off Texas. From light brown mud with almost black MnO layers near (within 20 cm of) the core tops, the downward transition is through a light olive grey mud with a variety and abundance of distinct mottles to a more homogeneous, light olive grey mud, to a relatively thin (5 - 25 cm) reddish zone, commonly with distinct chevron burrows within it or just below it, to a darker olive grey mottled mud. From a larger collection (>100) of cores from the Texas and western Louisiana slopes, fourteen radiocarbon dates from within or near the reddish zone indicate that its age is 12,000 B.P. This horizon is used herein as the Holocene/Pleistocene (H/P) boundary. Within this core suite, this boundary also correlates with a down-core decrease in carbonate content and a change to isotopically lighter organic carbon. Although porosities of hemipelagic sediments rarely drop below 75% within the upper 5 meters of core, a subtle decrease in porosity and/or

an increase in the rate of porosity loss from compaction also commonly occurs downward across the H/P boundary. All of the above characteristics assist in estimating the location of this chronostratigraphic horizon.

Table 2 summarizes accumulation rates based on the 12,000 B.P. horizon. It is identifiable in four cores from within the basin and one (89G1-5) from an immediately adjacent bathymetric high. Averages for a larger suite of 19 cores from the nearby Texas continental slope provide a perspective for the basin cores. Only thicknesses of hemipelagic muds were used. Intervening mass transport deposits (debrites) were considered to represent zero time and their thicknesses were excluded. The exclusion consisted of only one unit from core IG45-23.

On the bathymetric high (core 89G1-5) and steep basin margin (core IG45-25), accumulation rates are somewhat lower than the average value for the larger core suite. IG38-18 is from near the upper boundary of the lower basin margin zone and has the next highest accumulation rate (slightly above the larger average). The last two cores tabulated (IG45-23 and -24) are from within the lower basin margin but near the basin floor and show the highest accumulation rates of the small suite (and also of the larger suite). Thus there is a gradient in which the accumulation rates of Holocene hemipelagic mud increase (approximately double) from the steep upper basin margin to the lower margin at the basin floor.

Debrites

All cores from the lower basin margin (IG38-18, IG45-23, IG45-24, 89G1-1, 89G1-3, and 89G1-4) contain zones of highly contorted bedding. The beds are commonly discontinuous to the extent that pieces of beds become rounded into cobbles and pebbles. The units are described as mud pebble conglomerates. These are interpreted to be debrites formed by plastic (grain supported) flow (for illustrations of sedimentary structures see Woodbury, 1977, Fig. 5 and Woodbury et al., 1978, Fig. 7). Texturally, the debrites may have somewhat less fine clay (>10 phi) than the hemipelagic muds, but textural differences are small (Appendix A). Debrite porosities are usually below 75% (note Fig. 4).

The extent of debrites in cores from the lower basin margin is quite variable (from 2% to 97%); and the depth to the youngest debrite varies from 12 cm to almost 6 m (Table 3). The deeper debrites clearly occur below the H/P boundary, but the shallowest are well within the current period of high sea level. Ages of the shallowest debrites are estimated from accumulation rates of the overlying hemipelagites (Table 2) and shown in Table 3.

One of the types of pebbles that occur in the debrites is a massive black mud. In core 89G1-4 the frequency and size of these black pebbles increase downward, and at 225 cm, the base of the debrite lies on this mud. The only other debrites which do not conformably overlie hemi-

pelagic mud are two debrites from core 89G1-3 which overlie other debrites.

Turbidites

Only two cores (89G1-2 and L566-7) were recovered from the basin floor, but they contained a total of six or seven graded beds. The muddy upper portions of these beds have extremely uniformly smooth structure with no traces of the mottling typical of the hemipelagic muds. Texturally they are very slightly more clayey than the debrites and hemipelagites, because they are absolutely sand free (Appendix A). These are basically the same textures as thick unifites from intraslope basins on the western Louisiana continental slope (Behrens, 1984). These muds grade downward into basal foraminiferal sands with occasional small pebbles of the same textures and colors as occur in the mud pebble conglomerates. Turbidite thicknesses range from 6 to at least 72 cm and increase downcore. Relative to hemipelagic muds, carbonate content is high in the foram-rich bases and low in the sand-free turbidite muds (Fig. 4). Thicknesses of hemipelagic muds between turbidite beds range from 0 to 85 cm. This represents time intervals of roughly 0 to 4,000 years based on accumulation rates.

Multichannel data

Two 24 channel lines (CS5 and CS11, Fig. 1) show that the salt underlying the bathymetric highs on all sides of the basin actually penetrates to higher elevations than the basin floor (Fig. 5). As with many intraslope basins, strong, continuous seismic reflections and chaotic zones are repeated cyclically. The cyclicity is not so clearly developed as in some intraslope basins (e.g., Fig. 6), but it is clearly present, and the cycles are extraordinarily thick (~800 m), in fact, as thick as any observed in intraslope basins.

Discussion and Conclusions

Sedimentation Overview

The textures and compositions that the three sediment types within the basin have in common (fine clays and skeletal carbonate with very little, if any, coarse terrigenous clastics) show that the turbidites and debrites represent redeposition of hemipelagic mud. The steep basin margins are the sides of diapiric salt structures where, presumably, instability due to oversteepening leads to slumping and turbidity current formation. The grain supported debris flows stop (freeze) shortly after reaching the lower slope near the basin floor and deposit the debrites forming the lower basin margin facies. The fluid turbidity currents presumably flow across the entire, small basin floor and deposit turbidites more uniformly there.

Sediment sources

Debrites

The hypothesis that the steep basin margin is the source area for the debrites, is not supported with examples of erosion scars within the steep basin margin, but the data are poor for evaluating the distribution of erosion. The very steepness which promotes instability also precludes good acoustic imagery, especially with the track lines available, which are almost all sub-radial to the basin. Erosional troughs or cusps would be relatively difficult to detect in such longitudinal or highly oblique sections.

On the other hand, two cores show evidence of erosion within the lower basin margin - the debrite deposition region. The downward increase in abundance and size of black pebbles in core 89G1-4 (uppermost part of the lower basin margin zone on the basin's eastern side) clearly shows a debris flow 'frozen' as it was incorporating (eroding) the underlying black mud. The second example is from the lower part of the lower basin margin zone (on the basin's northern side). There, core 89G1-3 contains three debrites, the youngest from 12 to 280 cm, the oldest from 280 to 476 cm, and a thin wedge, only zero to five cm thick, between the other two. The thinness and angular surface of the intervening debrite suggests that much of it was eroded by the overriding debris flow and incorporated into its consequent debrite.

Erosion within the zone of deposition is intuitively unexpected, but the core evidence is supported by 3.5 kHz images of the debrites. Figure 7 shows that the core showing erosion by the most recently deposited debrite (~440 B.P., 89G01-3) was taken from a lobe of acoustically transparent material at least 16 m thick (minimum thickness is from using water column acoustic speed - 1500 m/s). The lower 12 m of this lobe appear to have replaced (eroded) the adjacent, flat-lying, basin floor sediments.

A further unanticipated implication of these observations is that what seems to be a single debrite lobe in the 3.5 kHz image, has, within a core therefrom, multiple debrite beds. The multiple beds suggest either multiple debris flow events or multiple flow layers within one event. The smooth oval continuity of the acoustic image, seemingly, would not be formed by multiple, separate events; so multiple layers of flow is offered as the working hypothesis.

Turbidites

Unquestionably, turbidity currents originated upslope from the basin floor. Pertinent questions are: where?, or how far upslope?, and to what extent do they represent partial fluidization of the debris flows vs. independent events? The inclusion of debrite pebbles in the bases of the basin floor turbidites suggests fluidization in connection with debrite formation. However, it might also be possible that turbidity currents originated higher on the slope and eroded some debrite on the way to the basin floor.

From the larger core suite cited earlier, long cores of hemipelagite usually have porosities below 75% only at core depths greater than 3 meters and commonly only deeper than 5 to 10 meters. Debrites, on the other hand, commonly range in porosity from 65 to 74% (average 69%), about 5% less porous than hemipelagites at equivalent depths (see Figure 4). Hence, the material within the debrites was presumably buried several meters before erosion and redeposition; and the more porous (>75%) muds which overlaid them are elsewhere (e.g., in the turbidites). If the more porous muds fluidize during debris flows and become turbidity currents that deposit turbidites on the basin floor, there should be close correlation in ages of debrite and turbidite tops in cores. Table 4 shows that the youngest debrite has no apparent correlative turbidite, but the next two older (deeper) debrites correspond very closely in age and/or depth with turbidites in the basin floor core. The second and third turbidites in the basin floor core have no intervening hemipelagite, so are considered as the same age. Indeed, they may be deposited from the same turbidity current that reflected from the basin wall and flowed back across the basin a second time. A short core from the western part of the basin floor suggests that the uppermost turbidite also consists of two graded beds in direct contact. The absence of a debrite corresponding to turbidite T4 could be simply the result of incomplete (cores not long enough) debrite sampling in the lower basin margin. It is concluded that at least some (and perhaps many or even all) basin floor turbidites result from fluidization associated with debris flows; and they may represent mostly the more porous mud previously overlying the material in the debrites.

Hemipelagites

The increasing depth of the reddish zone (used as the Holocene/-Pleistocene boundary), from the margin towards the center of the basin, indicates that perfectly uniform hemipelagic rain is not the sole source of the mottled mud interpreted to be hemipelagite. The occurrence of the lowest accumulation rate on the upper steep basin margin (core IG45-25, Table 2), - lower even than accumulation on the bathymetric high (core 89G1-5) - suggests differential deposition rates related not only to depth in the basin but also to the steepness of slope. However, the absence of any indication of erosional unconformities (e.g., scour surfaces in 3.5 kHz records or porosity discontinuities within cores) suggests that the loss is not by turbidity current or debris flow erosion but by resuspension. The mechanism for this resuspension should have the characteristics of high frequency (to be effective) and small scale (to be undetectable as discreet events). Two possibilities are offered for future working hypotheses. First, although the region is essentially aseismic, salt tectonism is obviously very active and may cause local microseisms that resuspend mud on diapir flanks. Second, warm core rings (at least one per year) are known to separate from the loop current and drift across the western Gulf (e.g.,

Cooper et al., 1990). This circulation may extend to the water bottom, especially with the large (200 - 400 km diameter) rings typical of the Gulf (Kelley and Weatherly, 1985; and Peggion and Weatherly, 1991), and randomly stir the highest porosity (>80%) surficial muds which would tend to resettle a little further downslope. For the aerial ratio of steep basin margin to the lower zones of debrite and turbidite deposition (7:3, Table 1), it would take a transfer of 23% of the hemipelagite from the upper to the lower part of the basin in order to double the rate of accumulation (Table 2).

Timing of salt movement

Assuming that debris flows are related to salt tectonism (i.e., are caused by uplift and oversteepening of slopes), the times of debris flow occurrence should reflect at least relative times of salt movement around the basin. From the observation that debrites lie deeper beneath hemipelagites in the western part of the basin and occur progressively shallower (stratigraphically higher) in a counterclockwise trend from the western to the northern margin (note Table 3), it can be interpreted that diapiric activity followed the same course.

Three debris flow events occur within the high sea level stand of the Holocene (Table 3) and suggest that there is a small lag between sediment loading (maximum at low sea level) and salt movement. This suggestion derives also from the observation in our large (~140) suite of cores from the slope that loading, represented by terrigenous clastic turbidite sands, occurs commonly below the H/P boundary but only quite rarely above it. For example, just upslope in the terminal basin of the downslope transport system described by Satterfield and Behrens (1990), numerous sands in three cores, all occur below the H/P boundary. The suggested association between sea level, sediment loading, and salt tectonism is supported slightly by the observation that the Holocene redeposition events within the basin occur sequentially younger from south to north (upslope) parallel to the direction of shoreline and depocenter shift during rising sea level. The predominance of hemipelagic deposition in the Holocene suggests that any lag is small, and redeposition is more active during times of low sea level.

Cyclic seismic stratigraphy and long term accumulation rates

The cyclic nature of slope sedimentation and, in particular, cyclic fill of intraslope basins connected to a shelf sediment source (note Figs. 5 and 6), typically has been attributed to cyclic sediment supply from the shelf, controlled, in turn, by cyclic sea level fluctuations (e.g., Bouma, 1981). The simplest hypothesis explaining the seismic cyclicity observed in the study basin, where isolation from shelf sediments implies purely salt tectonic control of gravity flow redeposition (and resulting thickening of basinal

sediments), is that sea level is the same ultimate control. There is only an additional step of salt movement responding to sediment loading. The loading would involve slope regions receiving shelf sediments (especially upslope), but it would also include the feedback of redeposition within the isolated basin itself.

A prediction from this hypothesis is that accumulation rates should be high during glacial stages (low stands, sediment loading and salt diapirism) and low during interglacial stages (high stands, hemipelagic sedimentation and salt quiescence). To test this, the three major (largest and shallowest) cycles observable in the seismic sections were tentatively correlated with three glacial/interglacial cycles (see Fig. 8) and, for comparison, with the third order sequences of Wornardt and Vail (1991). The strong parallel reflection seismic facies were interpreted as representing interglacial stages (like at present) when sedimentation in much of the basin consisted of alternating hemipelagites and thin turbidites, and debrites were mostly restricted to the basin margins. Chaotic seismic facies were interpreted as representing glacial stages when there was more active salt tectonism, and debris flows dominated sedimentation throughout the basin. The shallowest chaotic zone could be interpreted to contain three subcycles (Fig. 8) representing three 100,000 yr cycles or the three fourth order cycles (3.10.3, 3.10.2, and 3.10.1) of Wornardt and Vail (1991) and was assigned to the Wisconsinian. Earlier stages were assigned in order vertically downward through the section. Glacial and interglacial stage names used herein follow published Gulf Coast stratigraphy (e.g., Stude, 1984; Wornardt and Vail, 1991) where they are considered to represent generalized paleo-water depths (McFarlan and LeRoy, 1988).

Thicknesses are fairly well constrained by six velocity analyses from two multichannel lines through the basin. Thicknesses were converted to a constant porosity in order to avoid the distortion of shallower parts of the section appearing to accumulate more rapidly because of higher porosities. Porosities were calculated from the bulk density vs. depth curve derived by Nelson (1990; Fig. 7) from a large set of well data.

Figure 9 shows the results graphically. The interpreted Kansan and Wisconsinian glacial stages show high accumulation rates, and interpreted interglacial stages generally show lower accumulation rates. However, all but two of the 12 stages in Figure 8 A and B follow closely the relationship pointed out by Sadler (1993) that rates are inversely proportional to the time intervals during which they are measured. Without the two exceptions, the linear correlation coefficient between log of time and log of rate is 0.87. The significant exceptions are: 1) the interglacial Sangamonian in Lamb et al.'s (1987) time scale has a low accumulation rate, and 2) the glacial Kansan using McFarlan and LeRoy's (1988) time scale has a high accumulation rate. Although these observations agree with the prediction, the evidence is weak at best. This could be expected, because almost all of the time intervals contain more than one 100 ky cycle and many more of

the shorter astronomical cycles that glacial eustatic sea levels tend to follow. Thus there were probably many sea level changes within each interval.

Accumulation rates for sequences (Fig. 8C) show no bias with time interval (log-log correlation coefficient = 0.04) and offer some support to the other rate patterns by their broadly parallel trends. Again, this does not test the hypothesis well, because there is at least one and usually more 100 ky cycles including both low and high sea levels in each sequence.

Figure 10 shows a comparison of accumulation rates in the isolated basin with accumulation rates in nearby upperslope basins receiving significant shelf sediments (Fiduk and Behrens, 1993). The most surprising observation is that the rates are of quite similar magnitudes. The rates in the isolated basin are somewhat lower, but they are also calculated over somewhat longer time intervals, and the time interval effect shown by Sadler (1993) can account entirely for the apparently lower values. Figure 10 also illustrates that almost all of these rates are more than an order of magnitude higher than present hemipelagic accumulation rates. In order for mass transport of hemipelagites to account for the observed basinal sediment thicknesses, there must be an approximately ten-fold concentration of sedimentation within the basin.

The amount of hemipelagite which must be removed from the basin margins and bathymetric highs to accomplish a ten-fold concentration depends on the size of the source area. If only the steep basin margin is the source, nearly 75% of it must be transferred into the basin. If the source area is extended 5 km beyond the present basin margin, only 50% of the material therein would need to be transferred. This would be a radius of just twice that of the thick basin fill. Seismic data coverage is insufficient to evaluate thickness changes between correlative strata in the basin and on surrounding bathymetric highs, but it is clear that sections over salt are much thinner than the section in the basin. From these thickness differences, it does not seem unreasonable that something on the order of 60% of the drape over adjacent diapirs could be transferred to the basin. This would require the source area to extend less than 3 km beyond the present basin margin and the ratio of source to basin areas to be 5:1. The basin studied can be considered at the high end of the spectrum of cycle thicknesses of basin fill. Thus the scenario is reasonable (more easily accomplished) for many other basins with thinner cycles.

Summary

The midslope basin studied is presently isolated by diapiric salt structures from receiving shelf sediments. Yet within it, there is considerable thickening of basin fill. Some thickening of basin fill results from differential deposition of hemipelagic mud, but most results from transfer of hemipelagic muds into the basin by debris flows and turbidity

currents. Presumably these are caused by oversteepening basin margins which are the flanks of the confining salt structures. At present, debrites are restricted to a 2 - 5 km wide zone around a basin floor of alternating hemipelagites and turbidites. Erosion by debris flows within the debrite deposition zone is documented. Turbidites seem to result from partial fluidization of at least some debris flows. Timing of the most recent gravitational transfer processes has progressed around the basin counter-clockwise from the west to the north and extends well into the Holocene high sea level stand.

Seismic stratigraphic cycles characterize basin fill and are hypothesized to correlate with glacial/interglacial sea level cycles. The correlation suggests that low sea levels cause enhanced downslope transfer of shelf sediments; and although these do not get into the isolated basin, their loading causes nearby salt to move and thus trigger the debris flows and turbidity currents within the basin. Rather recent (~500B.P.) activity suggests some lag to this process, but overall, low stands are interpreted to be represented by thick chaotic seismic facies representing, in turn, basin-wide debrites. High stands are interpreted to be represented by more continuous, strong parallel reflections. These are not so well developed as in other basins, which may be due to the lag effect or higher order sea level fluctuations causing more debris flow activity during broadly interglacial stages.

It is surprising that the seismic cycles are as thick as those within basins receiving shelf sediment by downslope transfer. However, the thicknesses are not entirely unreasonable for the geography of this basin. Furthermore, this basin can be considered the high end-member of a spectrum of cycle thicknesses, and other interdomal basins may more easily fit the same model.

Acknowledgments

Data collection previous to 1983 was supported financially by a consortium of 13 oil companies. Field work between 1988 and 1991 was done on student training cruises supported by the University of Texas at Austin through the Institute for Geophysics. This report was prepared with financial support from Shell Development, Conoco, Exxon, and BP Petroleum. I thank Drs. Thomas A. Davies and Martin B. Lagoe for thoughtful reviews of the manuscript. Institute for Geophysics contribution no. xxxx.

References

Addy, S. K., and Behrens, E. W., 1980. Time of accumulation of hypersaline anoxic brine in Orca Basin. Mar. Geol., 37:241-252.

Behrens, E. W., 1980. On sedimentation rates and porosity. Mar. Geo., 35: M11-M16.

Behrens, E. W., 1984. Unifite muds in intraslope basin, northwest Gulf of Mexico. Geo-Marine Letters, 4: 227-233.

Bouma, A. H., 1981. Depositional sequences in clastic continental slope deposits, Gulf of Mexico. Geo-Marine Letters, 1: 105-110.

Bouma, A. H., 1983. Intraslope basin in northwest Gulf of Mexico: a key to ancient submarine canyons and fans. In: Watkins, J. S. and Drake, C. L. (Editors), Studies in Continental Margin Geology, American Association Petroleum Geologists Special Publication 34: 567-581.

Bouma, A. H. and Garrison, L. E., 1979. Intraslope basins, Gulf of Mexico. Geol. Soc. Am. Bull. (Abs. with programs) 1979 Annual Meeting, San Diego, p. 329.

Bouma, A. H., Smith, L. B., Sidner, B. R., and McKee, T. R., 1978. Intraslope basins in northwest Gulf of Mexico. In: Bouma, A. H., Moore, G. T., and Coleman, J. M. (Editors), Framework, Facies and Oil-Trapping Characteristics of the Upper Continental Margin: American Association Petroleum Geologists Studies in Geology 7: 289-302.

Bouma, A. H., Stelting, C. E., Coleman, J. M., Cremer, M., Droz, L. I., Meyer, A. W., Normak, W. R., O'Connell, S., Pickering, K. T., and Stow, D. A. V., 1986. Seismic stratigraphy and sedimentary processes in Orca and Pigmy basins, In: Initial Reports of the Deep Sea Drilling Project, 96: 563-576.

Cooper, C. A., Forristall, G. Z., and Joyce, T. M., 1990. Velocity and Hydrographic structure of two Gulf of Mexico warm-core rings. J. Geoph. Res., 95: 1663-679.

Fiduk, J. C. and Behrens, E. W., 1993. A comparison of Plio-Pleistocene to recent sediment accumulation rates in the East Breaks area, northwestern Gulf of Mexico, In: Armentrout, J. M., R. Bloch, H. C. Olson and B. F. Perkins (Editors), Rates of Geologic Processes, Fourteenth Annual Research Conference, Gulf Coast Section SEPM Foundation, pp. 41-55.

Kelley, E. A. and Weatherly, G. L., 1985. Abyssal eddies near the Gulf Stream. J. of Geophys. Res., 90: 3151-5155.

Lamb, J. L., Wornardt, W. W., Huang, T. C., and Dube, T. E., 1987. Practical application of Pleistocene eustacy in offshore Gulf of Mexico. Cushman Foundation for Foraminiferal Research, Special Publication 24: 33-39.

Martin, R. G. and Bouma, A. H., 1981. Active diapirism and slope steepening, northern Gulf of Mexico continental slope. Mar. Geotechnology, 5: 63-91.

McFarlan, E., Jr. and LeRoy, D. O., 1988, Subsurface geology of the late Tertiary and Quaternary deposits, coastal Louisiana and the adjacent continental shelf. Transactions Gulf Coast Association Geological Societies, 38: 421-433.

Nelson, T. H., 1991. Salt tectonics and listric-normal faulting. In: Salvador, A. (Editor), The Gulf of Mexico Basin. (The Geology of North America, J) Geol. Soc. Am., pp. 73-89

Peggion, G. and Weatherly, G. L., 1991. On the interaction of the bottom boundary layer and deep rings. Mar. Geol., 99: 329-342.

Sadler, P. M., 1993. Time scale dependence of the rates of unsteady geologic processes, In: Armentrout, J. M., R. Bloch, H. C. Olson and B. F. Perkins (Editors)., Rates of Geologic Processes, Fourteenth Annual Research Conference, Gulf Coast Section SEPM Foundation, pp. 221-228.

Satterfield, W. S. and Behrens, E. W., 1990. A late Quaternary canyon/-channel system, northwest Gulf of Mexico continental slope. Mar. Geol., 92: 51-67.

Stude, G. R., 1984. Neogene and Pleistocene biostratigraphic zonation of the Gulf of Mexico basin, In: Characteristics of Gulf Basin Deep-Water Sediments and Their Exploration Potential, Fifth Annual Research Conference, Gulf Coast Section SEPM Foundation, pp. 92-101.

Trabant, P. K., and Presley, B. J., 1978. Orca Basin, anoxic depression on the continental slope, northwest Gulf of Mexico, In: Bouma, A. H., Moore, G. T., and Coleman, J. M. (Editors), Framework, Facies and Oil-Trapping Characteristics of the Upper Continental Margin. American Association Petroleum Geologists Studies in Geology 7: 303-311.

Woodbury, H. O., 1977. Movement of sediment on the Gulf of Mexico, continental slope and upper continental shelf. Mar. Geotechnology, 2: 263-273.

Woodbury, H. O., Spotts, J. H., and Akers W. H., 1978. Gulf of Mexico continental-slope sediments and sedimentation, In: Bouma, A. H., Moore, G. T., and Coleman, J. M. (Editors), Framework, Facies and Oil-Trapping Characteristics of the Upper Continental Margin. American Association Petroleum Geologists Studies in Geology 7: 117-137.

Wornardt, W. W. and P. R. Vail, 1991. Revision of the Plio-Pleistocene cycles and their application to sequence stratigraphy and shelf and slope sediments in the Gulf of Mexico. Trans. Gulf Coast Assoc. Geol. Soc., 41: 719-743.

Table 1 Basin Facies

	steep basin margin (69%)		lower basin margin (25%)		basin floor (6%)	
	range	mean	range	mean	range	mean
width (km)	2.5 - 6.5	3.5	1.5 - 5.5	2.5	3.0 - 5.5	3.5
(n.mi.)	1.3 - 3.5	2.0	0.8 - 3.0	1.3	1.6 - 3.0	2.0
acoustic character*	I, VI or none		V		II	
sediments	hemipelagic mud		debrites & hemipelagites		turbidites & hemipelagites	

* I - sharp bottom echo with multiple, parallel subbottoms
II - sharp bottom echo with fewer (3 - 6) subparallel subbottoms
V - semiprolonged bottom echo with few if any subbottoms
VI - sharp bottom echo, no subbottoms

Table 2 Accumulation Rates for Hemipelagic Muds

Core depths in centimeters to Holocene/Pleistocene contact (12,000 B.P.)

DEPTHS		POROSITIES (%)*					
CORE ID	water (m)	core (cm)	in situ	75	63	30	setting
			accumulation rates (cm/ky)*				
89G1-5	1096	150	12.5	10.3	**6.5**	3.7	nearby bathymetric high
IG45-25	1318	124	10.3	8.6	**5.8**	3.1	steep basin slope
IG38-18	1724	170	14.2	11.9	**8.0**	4.3	upper, lower basin margin
IG45-23	1767	208	17.3	15.2	**10.0**	5.4	lower, lower basin margin
IG45-24	1763	260	21.7	18.4	**12.4**	6.6	lower, lower basin margin
mean (5)		187	15.6	13.2	**8.8**	4.6	
st.dev. (5)		57	4.7	4.2	2.9	1.4	
mean (19)		151	12.9	11.1	**8.2**	4.1	nearby Texas
st.dev. (19)		52	3.9	3.9	2.8	1.2	continental slope

* Four rates are for four porosities to facilitate comparison with other data sets. The variable porosities of in situ data; constant porosities of: 75% - decompacted to ≈depositonal value, 63% - thickness values equal mass values of gm/cm^2, and 30% - approximately the compacted thicknesses at 1500m - for comparison with observations from seismic sections.

Table 3 Estimated Ages of Youngest Debrites

depth - water depth in meters; length - total core length in centimeters; abundance - number of debrites and percentage of core; top - depth in core to top of shallowest debrite; est age - years before present calculated by dividing depth to top of unit by estimated Holocene accumulation rate. Cores ordered by decreasing age of shallowest debrite also turn out to be in counterclockwise order around the basin from west to north.

CORE	depth meters	length cm	abundance # - %	top cm	est age years B.P.	locations	
IG45-24	1763	768	2 - 7%	595	**33,000**	lower, lower margin	**West**
IG38-18	1724	960	2 - 2%	186	**13,200**	upper, lower margin	**WSW**
IG45-23	1767	743	2 - 47%	208	**12,000**	lower, lower margin	**SW**
89G1-1	1760	286	1 - 57%	124	**5,470**	mid, lower margin	**South**
89G1-4	1730	394	1 - 52%	23	**1,100**	upper, lower margin	**East**
89G1-3	1765	476	3 - 97%	12	**440**	lower, lower margin	**North**

Table 4 Correspondence between debrites and turbidites

CORE	depth to top of first debrite (cm)	depths to turbidite tops in core 89G1-2 (cm of hemipelagite)	calculated ages* (B.P.) debrite	turbidite
89G1-3	12	none	440	none
89G1-4	23	22 (T1)	1,100	960
89G1-1	124	117 (T2 & T3)	5,470	5,410
		139 (T4)	none	6,510

* ages are based on a hemipelagite accumulation rate of 12 cm/1000 yrs (typical of the rates at the lowest basin margin; see Table 2) at a constant porosity of 63%.

Table 5 Estimated accumulation rates for seismic sequences shown in Figure 8

depth (m)**	P %***	redepths* (m) at new porosity (%) 63	75	30	T^ kyr	ΔT kyr	accumulation rates in situ cm/kyr	63% (x10 = m/ma)	75%	30%	stage (picked at bases of seismic strat. cycles)
2	75	1	2	1	12	12	16.7	11.3	16.7	5	Holocene^^
702	37.0	834	1234	441	300	288	243	289	428	153	Wisconsinan
891	34.9	1161	1718	614	420	120	158	273	404	144	Sangamonian
1460	30.2	2198	3253	1162	850	430	132	241	357	128	Illinoian
1730	28.5	2714	4016	1434	1450	600	45	86	127	45	Yarmouthian
2726	23.6	4705	6963	2487	1600	150	664	1327	1965	702	Kansan
2939	22.7	5147	7618	2721	2250	650	33	68	101	36	Aftonian

* calculated according to Behrens (1980)
** converted from six velocity structure analyses on two multichannel lines through the basin
*** porosities derived from Nelson (1991)
^ from Lamb et al. (1987)
^^ from piston cores (this study)

depth (m)**	P %***	redepths* (m) at new porosity (%) 63	75	30	T^ kyr	ΔT kyr	accumulation rates in situ cm/kyr	63% (x10 = m/ma)	75%	30%	stage (picked at bases of seismic strat. cycles)
2	75	1.35	2.00	0.71	12	12	16.7	11.3	16.7	5	Holocene^^
702	37.0	834	1234	441	195	183	383	455	673	240	Wisconsinan
891	34.9	1161	1718	614	650	455	42	72	106	38	Sangamonian
1460	30.2	2198	3253	1162	1200	550	103	189	279	100	Illinoian
1730	28.5	2714	4016	1434	1450	250	108	206	305	109	Yarmouthian
2726	23.6	4705	6963	2487	1850	400	249	498	737	263	Kansan
2939	22.7	5147	7618	2721	2250	400	53	111	164	58	Aftonian

^ from McFarlan and LeRoy (1988)

depth (m)**	P %***	redepths* (m) at new porosity (%) 63	75	30	T^ kyr	ΔT kyr	accumulation rates in situ cm/kyr	63% (x10 = m/ma)	75%	30%	stage (picked at bases of seismic strat. cycles)
2	75	1	2	1	12	12	16.7	11.3	16.7	5	Holocene^^
702	37.0	834	1234	441	300	288	243	289	428	153	3.10.
891	34.9	1161	1718	614	500	200	94	164	242	86	3.9, 3.9.5 & 3.9.6
1460	30.2	2198	3253	1162	1100	600	95	173	256	91	3.9, 3.9.1-3.9.4
1730	28.5	2714	4016	1434	1400	300	90	172	254	91	3.8, 3.8.2
2726	23.6	4705	6963	2487	1900	500	199	398	589	210	3.8, 3.8.1
2939	22.7	5147	7618	2721	2400	500	43	88	131	47	3.7, 3.7.3

^ from Wornardt & Vail (1991)

FIGURE CAPTIONS

Figure 1 Index Map. Bathymetric map showing positions of bathymetric highs (+) and lows (-). Intraslope basins are labelled I, II, III, IV, V, Gyre, and Horshoe. Basins I - III are sediment filled. Basins I - IV are connected by a series of canyons and channels (dots and dashes) and are the downslope sediment transport system documented by Satterfield and Behrens (1990). Basin V is the isolated inter-domal intraslope basin of this study. Contour interval is 200 m. Modified from Satterfield and Behrens (1990, Fig. 1).

Figure 2 Study Area. A. Control: track lines and core locations. Heavier lines with labels are shown in other figures (e.g., multichannel lines CS5 and CS11). Dashed line is the primary coring cruise 89G01. B. Facies based on bathymetry and 3.5 kHz acoustic reflection patterns. Hemipelagites occur in all three facies; mud pebble conglomerates and turbidites are restricted to lower basin margin and basin floor facies respectively.

Figure 3 Basin Cross Section. 3.5 kHz profile showing the three acoustic facies and projected core locations. The profile goes through the site for core 89G01-3. Sites of cores 89G01-2, -1, and -4 are off line by 650, 1130, and 2090 m respectively. From cruise IG1603. Note Appendix B for additional 3.5 kHz basin cross sections.

Figure 4. Porosities vs. depth in core for debrites and hemipelagites. Overlap may be due, in part, to textural differences. Porosity differences suggest that material in debrites was buried at least 3 meters before redeposition.

Figure 5. Multichannel lines through the study basin. Location of lines is shown in Figure 2.

Figure 6. Multichannel line showing exceptionally well developed cyclicity of seismic facies.

Figure 7. 3.5 kHz profile (A) and line drawing (B) of debrite lobe in contact with the basin floor. From cruise 89G01.

Figure 8 Interpreted Pleistocene stratigraphy in isolated basin. W - Wisconsinian, s-Sangomonian, i - Illoian, y - Yarmouthian, k - Kansan, a - Aftonian. Line is CS5 shown in Figure 5.

Figure 9. Accumulation rates based on interpreted correlation of observed seismic cycles with major Pleistocene stages or third and fourth order seismic sequences. See Table 5 for data and more details.

Figure 10. Accumulation rates in isolated basin compared with those in basins receiving shelf sediment and with Holocene hemipelagic rates determined from a large suite of piston cores form the slope.

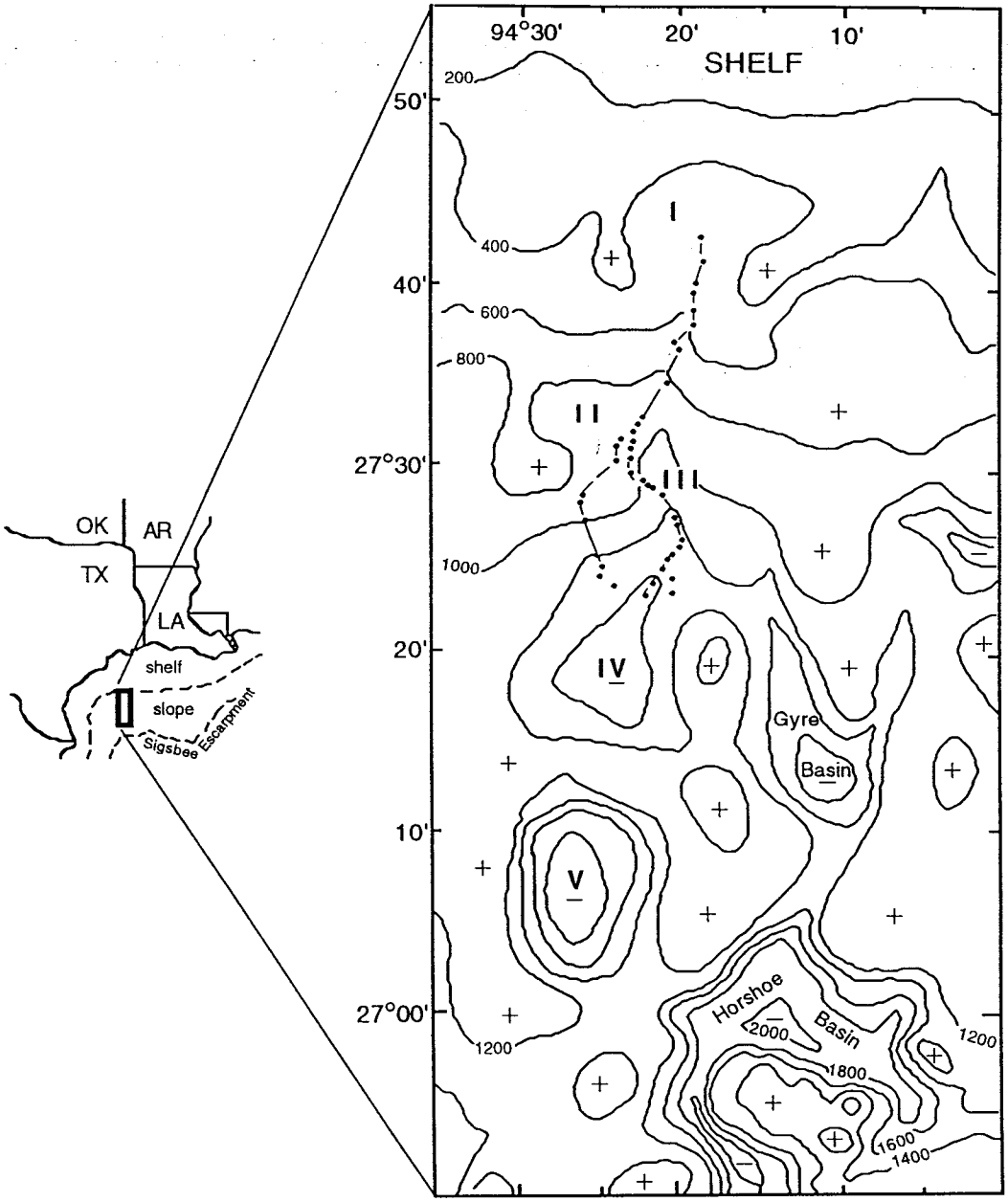
94°30'
20'
10'
SHELF
200
50'
400
40'
600
800
27°30'
1000
20'
10'
27°00'
1200
I
II
III
IV
V
Gyre
Basin
Horshoe
Basin
2000
1800
1600
1400
1200
OK
AR
TX
LA
shelf
slope
Sigsbee Escarpment

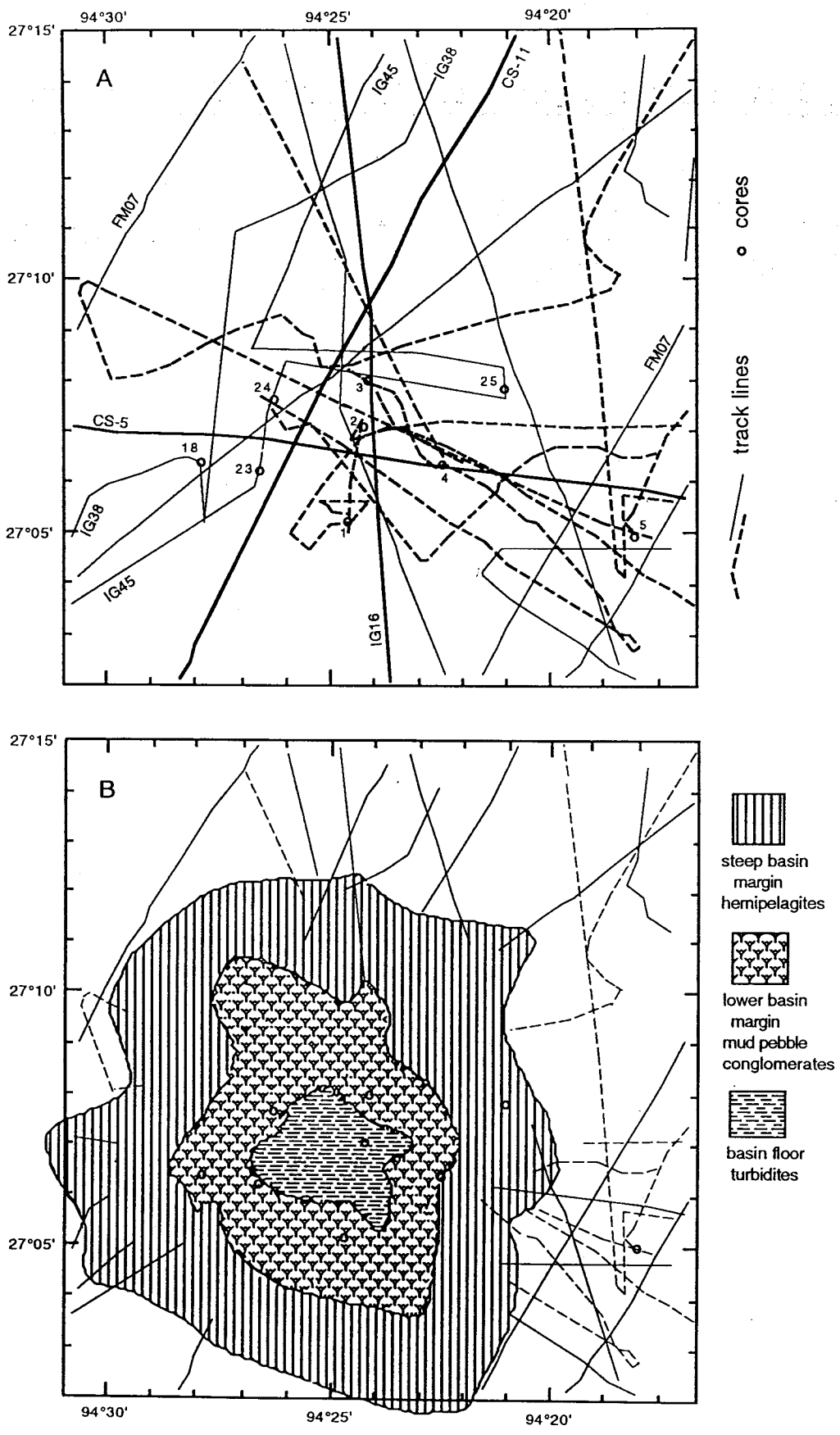
A
B
94°30'
94°25'
94°20'
27°15'
27°10'
27°05'
FM07
IG45
IG38
CS-11
CS-5
IG16
1
2
3
4
5
18
23
24
25
cores
track lines
steep basin margin hemipelagites
lower basin margin mud pebble conglomerates
basin floor turbidites

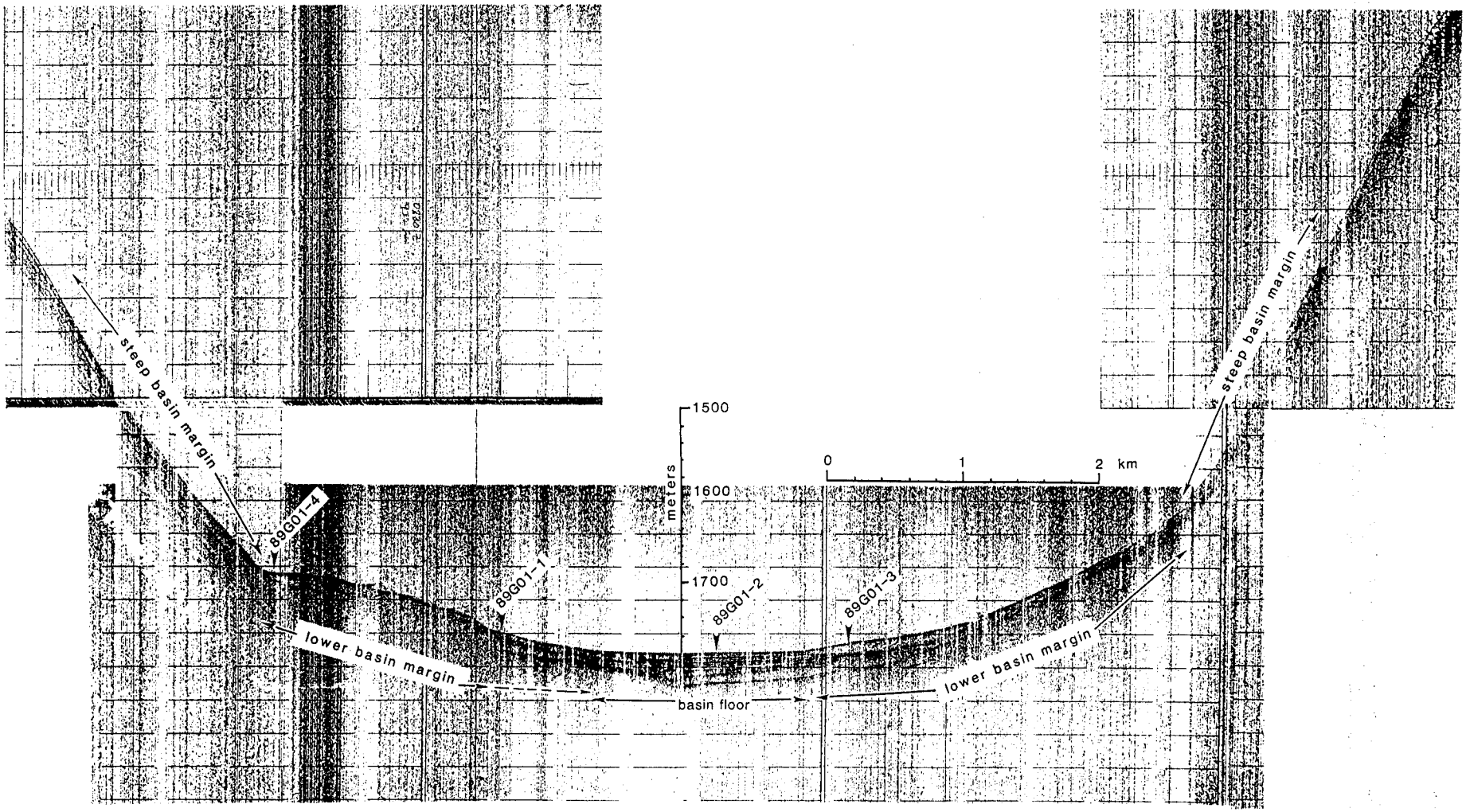
steep basin margin
89G01-4
89G01-1
89G01-2
89G01-3
lower basin margin
basin floor
lower basin margin
steep basin margin
1500
1600
1700
meters
0
1
2 km

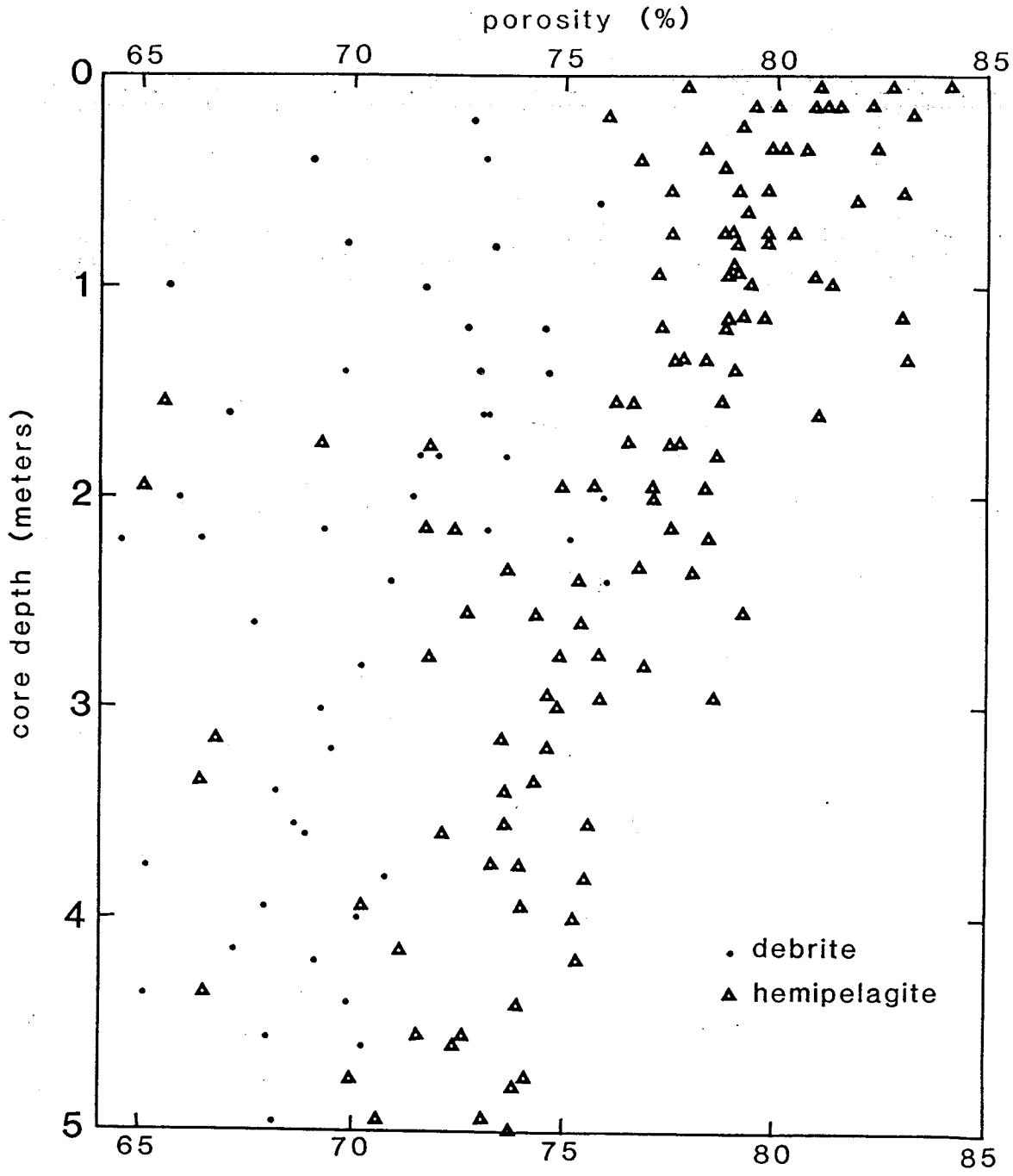
porosity (%)
65
70
75
80
85
0
1
2
3
4
5
core depth (meters)
debrite
hemipelagite

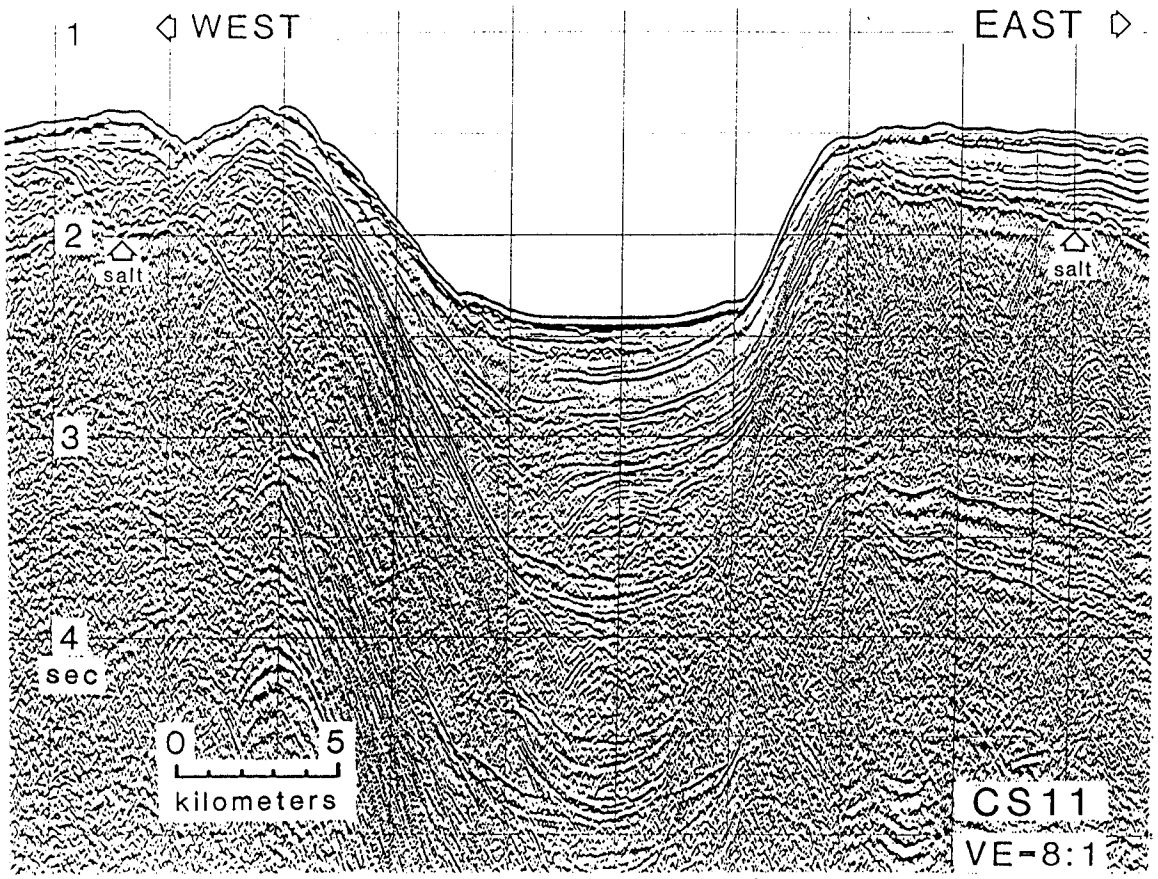
1
WEST
EAST
2
salt
salt
3
4
sec
0
5
kilometers
CS11
VE-8:1

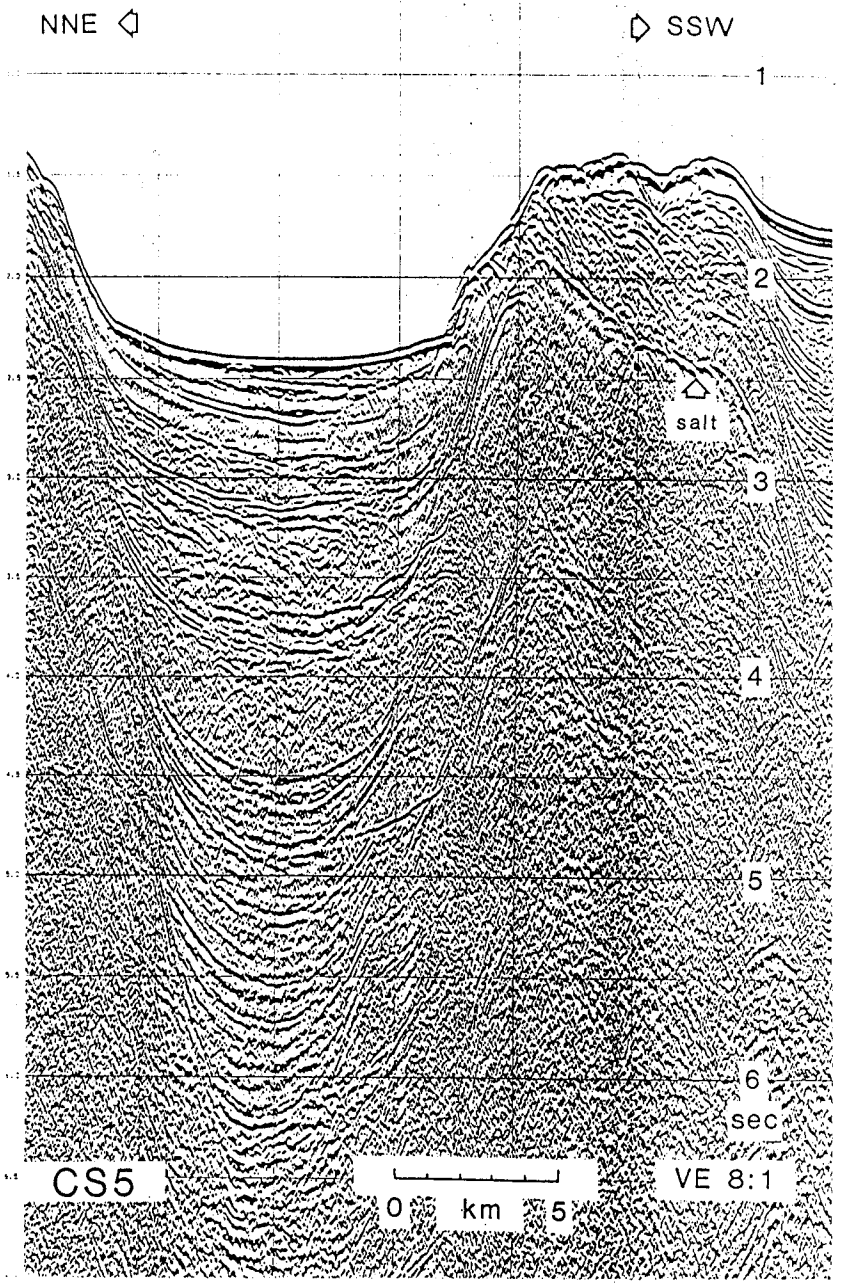
NNE
SSW
1
2
salt
3
4
5
6
sec
CS5
0
km
5
VE 8:1

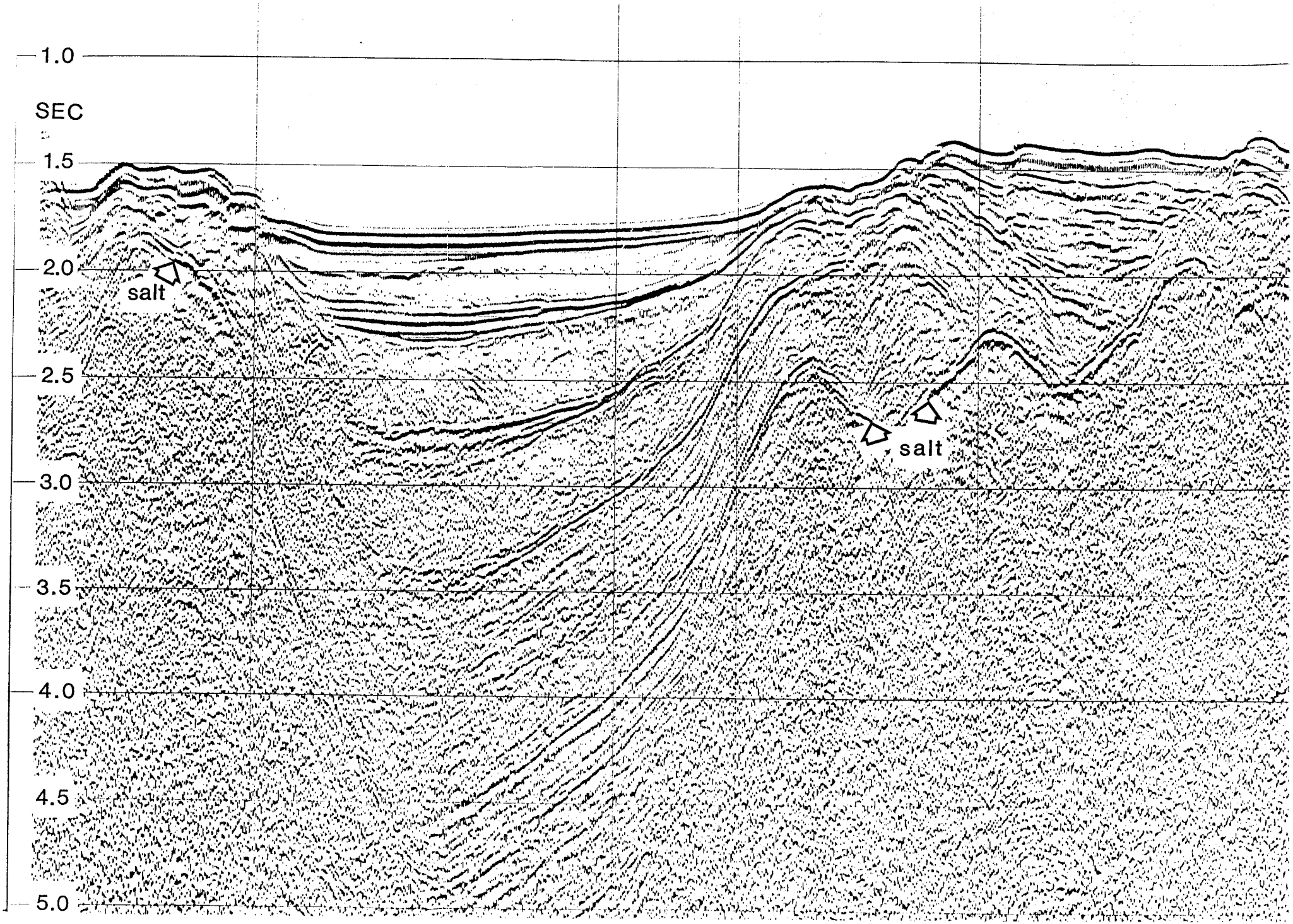
1.0
SEC
1.5
2.0
salt
2.5
salt
3.0
3.5
4.0
4.5
5.0

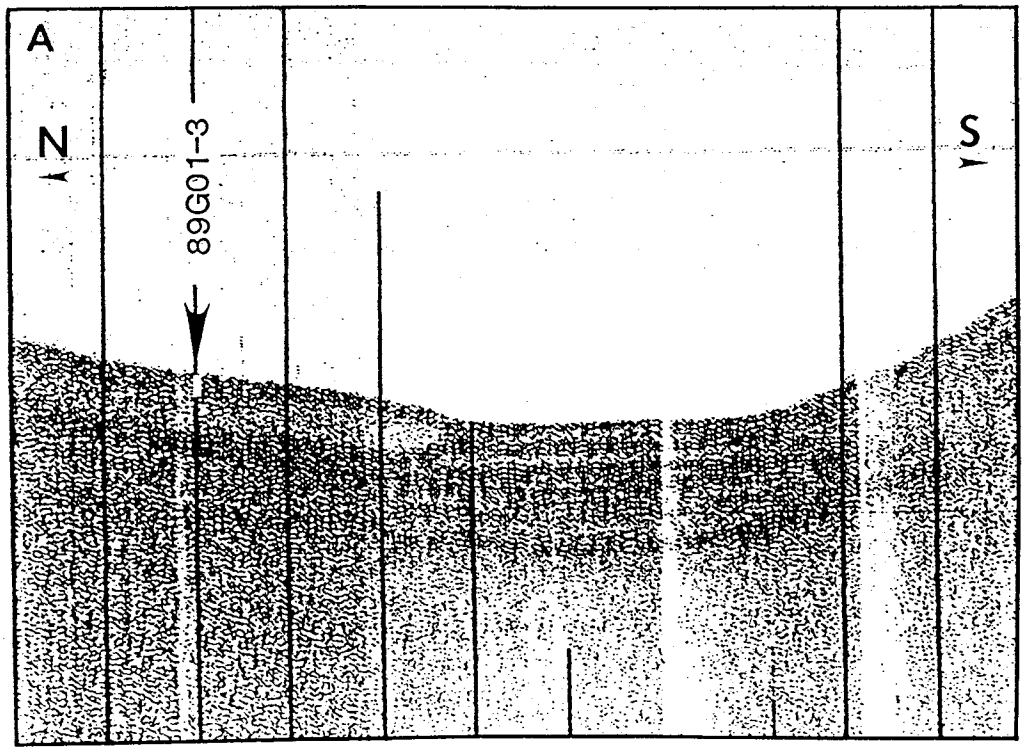
A
N
89G01-3
S

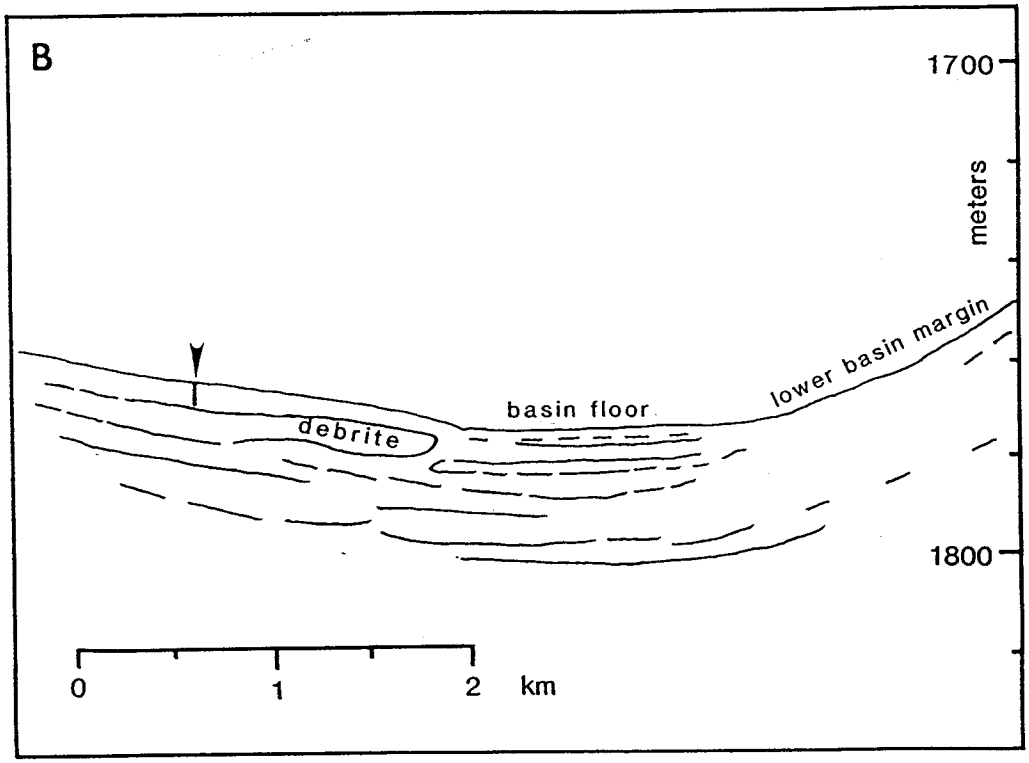
B
1700
meters
lower basin margin
basin floor
debrite
1800
0
1
2
km

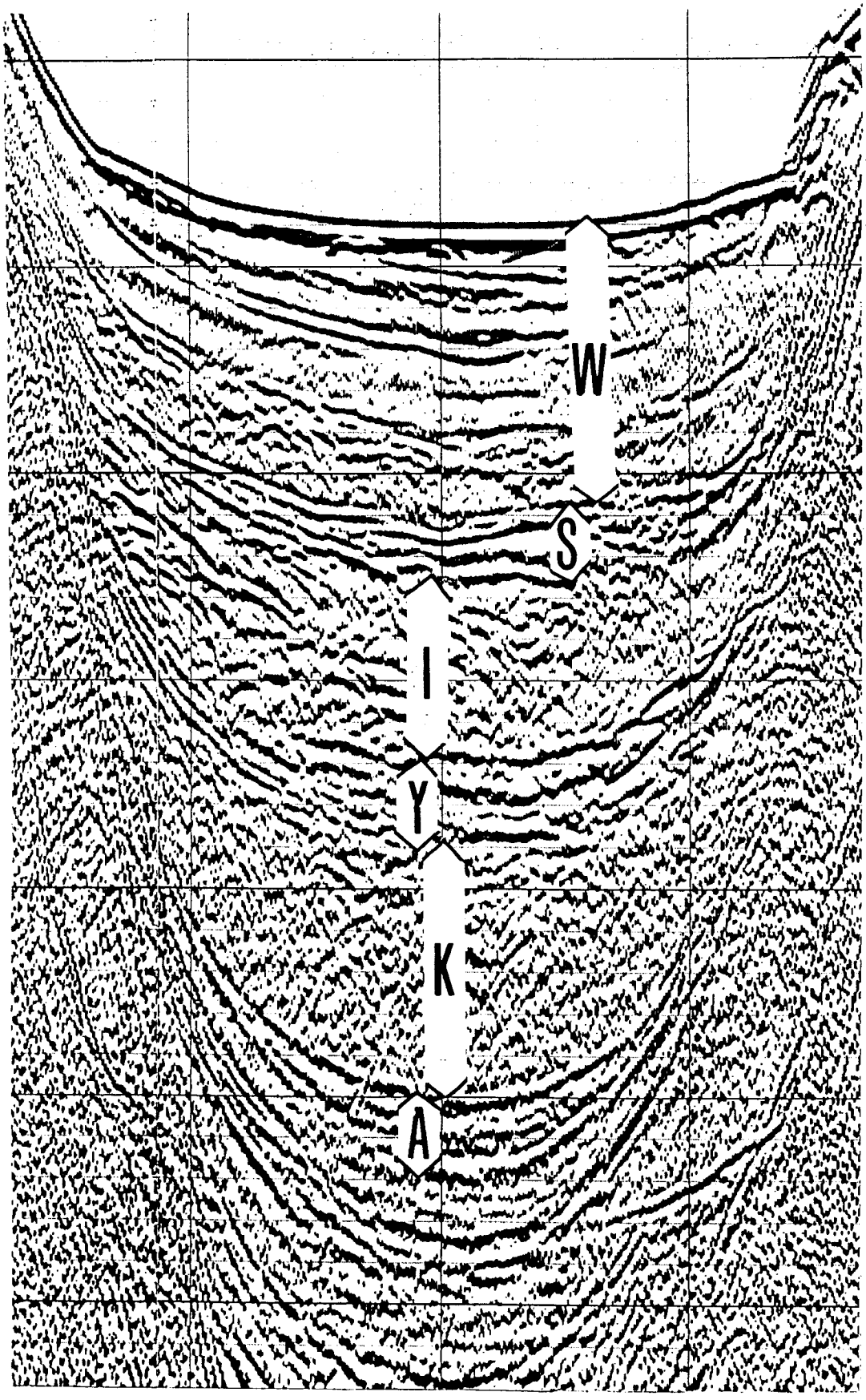
W
S
I
Y
K
A

ACCUMULATION RATES IN ISOLATED INTERDOMAL BASIN

W - Wisconsinian, S - Sangamonian, I - Illinoian,
Y - Yarmouthian, K - Kansan, A - Aftonian;
— heavy outline - *in situ* porosities;
patterns - constant porosities (30%)

A - stages after Lamb et al., 1987

B - stages after McFarlan & LeRoy, 1988

C - third & fourth order sequence cycles of Wornardt & Vail, 1991

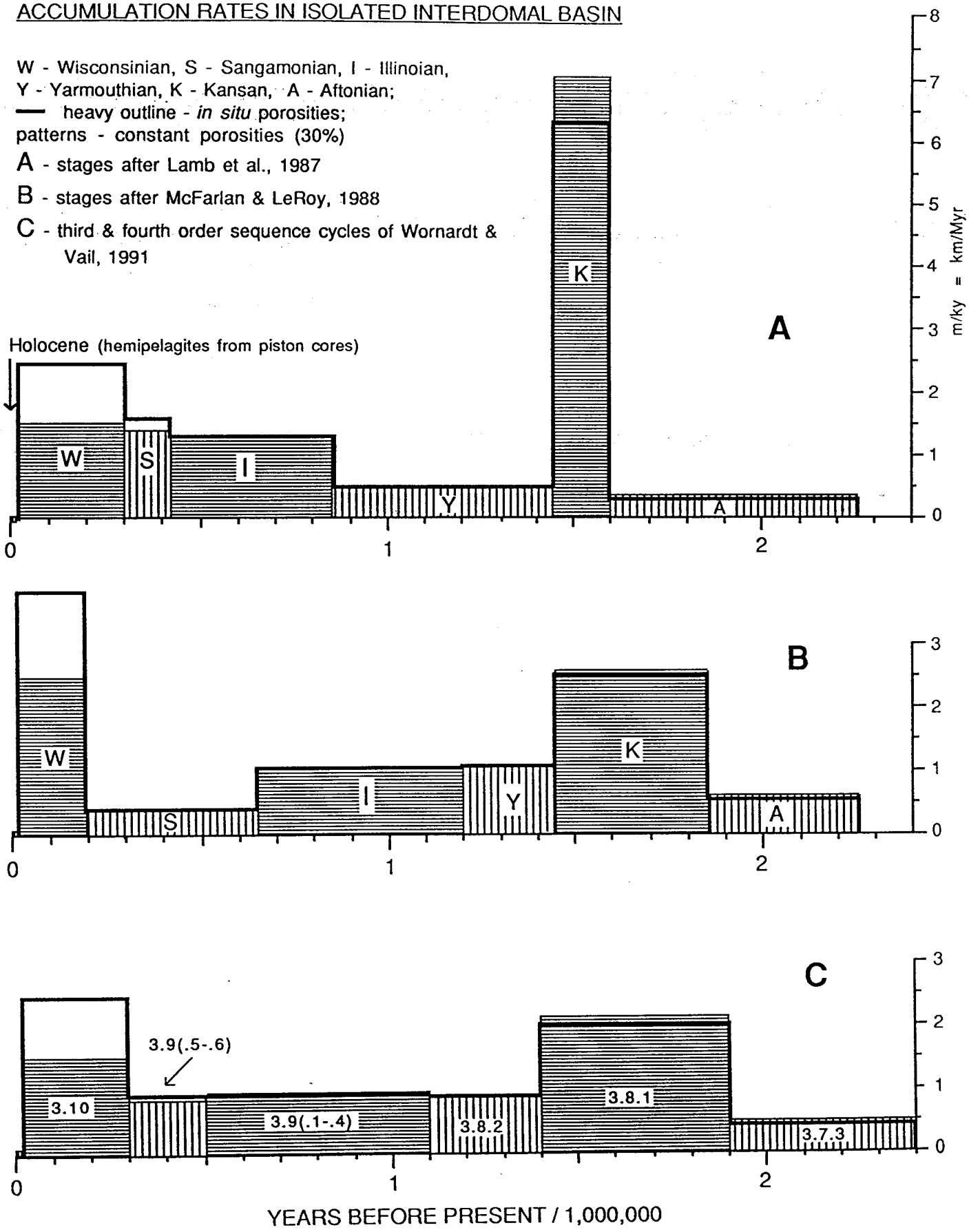

CONTINENTAL SLOPE ACCUMULATION RATES
NORTHWESTERN GULF OF MEXICO

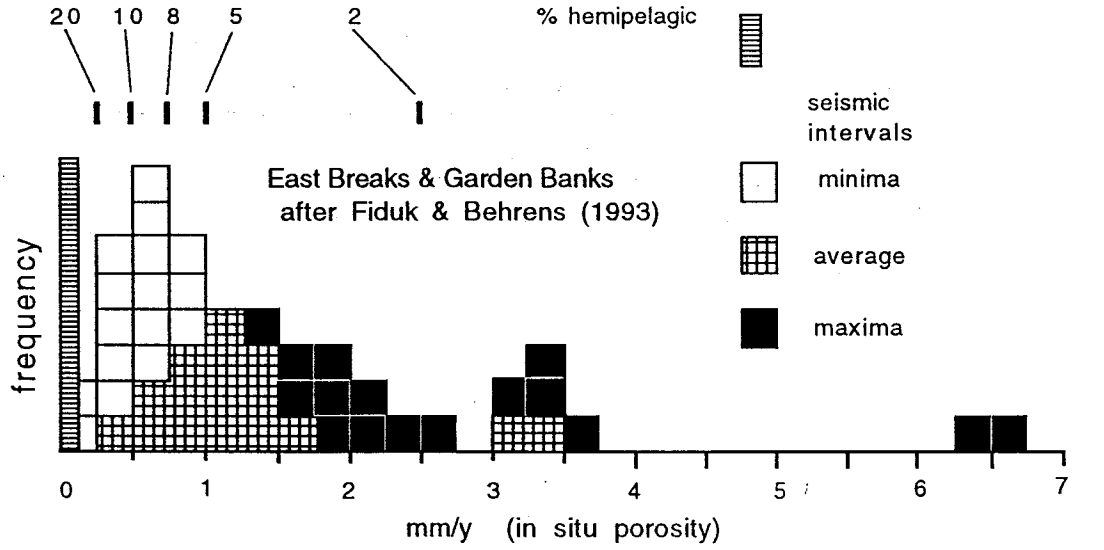

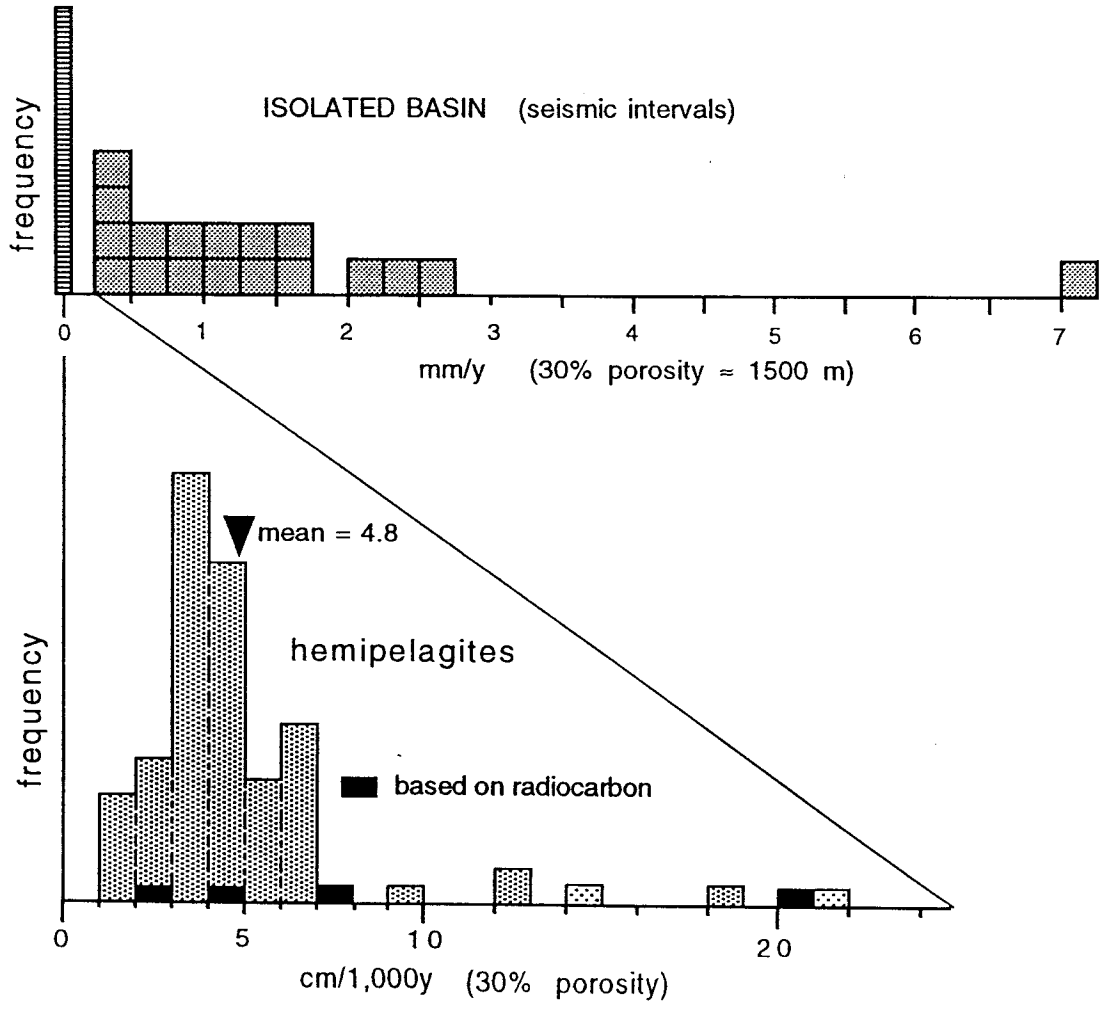

APPENDIX A TEXTURES

Core locations are shown in Figure 2a (by core number). Unifites are for comparison with turbidites, note lack of sand; locations: IG45-7 - 27°26.0'N, 90°44.6'W; IG45-8 - 27°31.2'N, 90°55.3'W. Depths are in centimeters from the core top. HP mud - hemipelagic mud; st cl - silt/clay ratio; fcl - fine clay (>10phi); fcl cl - fine clay / total clay ratio; mode is phi range of mode or phi size of mean. Porosity is %. See text for further discussions.

cruise ID-core #	depth	sed type		sand	silt	clay	st cl	fcl	fcl cl	mode	porosity
89G1-1	60-80	HP mud		5.3	11.6	83.1	0.14	58.6	0.71	10-11	81
89G1-2	110-30	HP mud		5.6	13.6	80.8	0.17	56.3	0.70	10-11	76
89G1-5	40-60	HP mud		8.1	3.9	88.0	0.04	56.4	0.64	9-10	82
89G1-5	170-90	HP mud		2.8	15.7	81.6	0.19	55.3	0.68	9-11	81
89G1-5	290-310	HP mud		2.1	16.7	81.2	0.21	53.0	0.65	9-10	78
89G1-5	440-60	HP mud		4.1	11.5	84.3	0.14	56.0	0.66	9-10	76
IG38-18	40-60	HP mud		1.9	14.8	83.3	0.18	58.6	0.70	10.3	78
IG38-18	310	HP mud		2.6	13.7	83.7	0.16	59.3	0.71	10.3	70
IG38-18	350-60	HP mud		1.2	12.6	86.2	0.15	61.4	0.71	10.5	70
IG38-18	395	HP mud		3.0	13.2	83.8	0.16	59.6	0.71	10.3	71
IG38-18	690	HP mud		4.2	16.8	79.0	0.21	57.9	0.73	10.1	68
IG38-18	755	HP mud		4.3	15.0	80.7	0.19	59.6	0.74	10.1	68
IG38-18	800	HP mud		1.4	12.4	86.3	0.14	61.4	0.71	10.5	68
IG45-23	200	HP mud		0.6	17.9	81.5	0.22	60.0	0.74	10.3	75
IG45-24	50-60	HP mud		1.1	12.8	86.1	0.15	64.4	0.75	10.5	80
IG45-24	150	HP mud		1.3	14.2	84.5	0.17	63.3	0.75	10.4	77
IG45-24	200	HP mud		1.3	18.5	80.2	0.23	58.3	0.73	10.2	78
IG45-24	248-52	HP mud		0.7	9.4	89.9	0.10	67.2	0.75	10.7	79
IG45-25	40-50	HP mud		2.5	13.5	84.0	0.16	59.1	0.70	10.3	79
IG45-25	130-40	HP mud		1.1	12.6	86.4	0.15	65.4	0.76	10.6	78
IG45-25	280-300	HP mud		1.3	13.7	85.1	0.16	59.8	0.70	10.4	75
	279		means:	[2.7]	[13.5]	[83.6]	[.15]	[59.6]	[.71]		[76]
			st.devs.	(1.9)	(3.1)	(2.9)	(.04)	(3.4)	(.03)		(5)
	cm			%	%	%				Ø	%
89G1-1	220-40	debrite		2.9	14.6	82.5	0.18	58.9	0.71	10-11	76
89G1-3	90-110	debrite		2.4	13.0	84.5	0.15	58.1	0.69	9-11	72
89G1-3	390-410	debrite		2.3	15.9	81.8	0.19	56.2	0.69	9-10	70
89G1-4	120-40	debrite		4.5	17.8	77.7	0.23	52.3	0.67	9-11	74
IG45-23	380-420	debrite		1.0	14.7	84.3	0.17	62.8	0.74	10.3	67
IG45-23	590-610	debrite		0.9	29.2	69.9	0.42	47.1	0.67	9.7	62
IG45-24	580-90	debrite		0.1	27.5	72.5	0.38	48.1	0.66	9.8	63
	349		means:	[2.0]	[19.0]	[79.0]	[.25]	[54.7]	[.69]		[69]
			st.devs.	(1.5)	(6.6)	(5.8)	(.11)	(5.8)	(.03)		(5)
	cm			%	%	%				Ø	%
89G1-2	220-40	turbidite		0.0	13.0	87.0	0.15	58.6	0.67	9-10	77
89G1-2	320-40	turbidite		0.0	16.0	84.0	0.19	58.3	0.69	11-12	77
	cm			%	%	%				Ø	%
IG45-7	150	unifite		0.1	12.2	87.8	0.14	73.9	0.84	10.9	77
IG45-7	350	unifite		0.0	12.0	88.0	0.13	64.7	0.74	10.6	77
IG45-7	500	unifite		0.0	10.2	89.8	0.11	63.5	0.71	10.7	74
IG45-7	650	unifite		0.0	15.3	84.7	0.18	58.2	0.69	10.4	72
IG45-8	300	unifite		0.0	15.2	84.8	0.18	55.0	0.65	10.3	75
IG45-8	550	unifite		0.0	7.6	92.4	0.08	64.0	0.69	10.8	74
IG45-8	800	unifite		0.0	12.2	87.8	0.14	59.2	0.67	10.5	71
IG45-8	1050	unifite		0.1	13.8	86.1	0.16	59.0	0.69	10.5	69
	544		means:	[0.0]	[12.3]	[87.7]	[.14]	[62.2]	[.71]		[74]
			st.devs.	(0)	(2.6)	(2.6)	(.03)	(5.8)	(.06)		(3)
	cm			%	%	%				Ø	%
89G1-4	240-60	black mud		0.7	14.3	85.0	0.17	63.1	0.74	10-11	62
89G1-4	340-60	black mud		0.0	30.5	69.5	0.44	46.6	0.67	10-11	54